

EXPERIMENTAL CHARACTERIZATION OF THE NONLINEAR RHEOLOGY OF ROCK

G. N. Boitnott

New England Research, Inc.
76 Olcott Drive, White River Junction, VT 05001, USA

ABSTRACT

The results of experiments on Berea sandstone are used to develop and constrain a rheological model for nonlinear deformation during arbitrary loading paths. An experimental protocol is illustrated which provides detailed constraint of the nonlinear deformation subject to arbitrary perturbations in axially symmetric compressive stresses. A second protocol is shown which addresses differences between moderate-strain static and small-strain dynamic measurements of elastic constants. Both stress amplitude and mode of deformation (loading path) are shown to significantly effect inferred elastic constants at low effective stresses.

KEYWORDS

Nonlinear Rheology, Mechanical Properties, Elastic Moduli, Velocities, Berea sandstone, Laboratory Tests, Deformation

INTRODUCTION

Many applications in geophysics involve the assumption that rocks deform as linear elastic materials. Analyses of seismic wave propagation, measurements and predictions of in-situ stresses, and predictions of stresses for a wide variety of geotechnical applications (such as borehole stability), all commonly involve assumptions of linear elastic deformation. However, from laboratory studies, it is well known that rocks rarely conform to this assumption.

Previous work on nonlinear, hysteretic rheologies has largely been based on experiments covering limited stress conditions and modes of deformation. These experiments have been important in guiding model development, having lead to an understanding of important qualitative features such as stress dependent moduli [Gorbatsevich 1996], stress amplitude dependence and hysteresis [McCall *et al.*, 1996], discrete memory (Boitnott, [1993] and Guyer *et al.* [1995]), and stress induced anisotropy [Johnson and Rasolofosaon, 1996]. Laboratory observations of the effects of nonlinearities indicate that they are persistent even for small stress perturbations (see Johnson *et al.*, [1993]), and thus the commonly made assumptions of linear elasticity should be critically evaluated.

Here we describe the results of laboratory experiments aimed at characterizing the rheology of rocks subject to moderate stresses. A sample of Berea sandstone is subjected to a series of perturbations in stresses. Perturbations in mean stress, differential stress, shear stress, and uniaxial strain are performed at a series of initial stress conditions. The stress-strain response exhibits considerable nonlinearity and hysteresis. From such data, a general rheological model is constructed which allows for predictions of stresses and strains during arbitrary loading paths. Comparisons of apparent static and dynamic elastic

constants are made and analyzed in the context of the developed nonlinear rheology.

DEFINITIONS AND APPROACH

The goal is to develop a model capable of predicting the stress-strain relationship for arbitrary loading paths for axially symmetric compressive stresses. Intuition leads us to try to formulate a rheology in terms of the mean stress (σ), the shear stress (τ), the volumetric strain (κ), and the shear strain (γ), defined as:

$$\sigma = (\sigma_{11} + 2\sigma_{\theta\theta})/3.0 \quad (1a)$$

$$\tau = (\sigma_{11} - \sigma_{\theta\theta})/2.0 \quad (1b)$$

$$\kappa = \varepsilon_{11} + 2\varepsilon_{\theta\theta} \quad (1c)$$

$$\gamma = \varepsilon_{11} - \varepsilon_{\theta\theta} \quad (1d)$$

where σ_{11} and $\sigma_{\theta\theta}$ are the axial and circumferential stresses and ε_{11} and $\varepsilon_{\theta\theta}$ are the axial and circumferential strains, respectively.

For an isotropic, linear elastic solid, $\kappa = \sigma/K$ and $\gamma = \tau/G$, where K and G are the bulk and shear elastic constants, respectively. Here the definitions of the elastic constants are generalized (and referred to as moduli) to allow for the description of nonlinear, hysteretic deformation. We define the more general bulk and shear moduli (\hat{K} and \hat{G}) to be:

$$\hat{K} = \frac{\partial\sigma}{\partial\kappa} \quad ; \quad \hat{G} = \frac{\partial\tau}{\partial\gamma} \quad (2)$$

Subscripts are used to distinguish between moduli measured from different loading paths. Loading paths and their associated subscripts are as follows: mean stress (σ), shear stress (τ), uniaxial stress (us), and uniaxial strain ($u\varepsilon$). Elastic moduli inferred from compressional and shear velocities (assuming isotropy and linear elasticity) are denoted by the subscript (v). Other common moduli are also discussed, but unlike \hat{K} and \hat{G} , are defined only for specific loading paths. These moduli include Young's modulus ($\hat{E}_{us} \equiv \partial\sigma_{11}/\partial\varepsilon_{11}|_{\Delta\sigma_{\theta\theta}=0}$) and the uniaxial strain modulus ($\hat{Y}_{u\varepsilon} \equiv \partial\sigma_{11}/\partial\varepsilon_{11}|_{\Delta\varepsilon_{\theta\theta}=0}$). In similar fashion, a generalized Poisson's ratio ($\hat{\nu}_{us} \equiv -\partial\varepsilon_{\theta\theta}/\partial\varepsilon_{11}|_{\Delta\sigma_{\theta\theta}=0}$) is also used. Parameters denoted without the ($\hat{\quad}$) represent values inferred from other parameters assuming isotropic, linear elasticity (e.g. $E_{\sigma\tau}$ is the inferred Young's modulus derived from measurements of \hat{K}_{σ} and \hat{G}_{τ}). The superscript ($'$) is used to denote the value of a parameter measured immediately after a reversal and loading direction, and symbols enveloped in $\langle \rangle$ denote the average value of the enveloped parameter over an extended range of loads (such as over an entire loading and unloading cycle).

EXPERIMENTAL PROCEDURE

Tests were performed in a hydraulically servo-controlled triaxial apparatus with a precision internal load cell in the loading column. Samples were all "room dry" Berea sandstone cored perpendicular to bedding, consisting of either 44.4 mm diameter or 25.4 mm diameter right cylinders with lengths equal to twice the diameter. Samples were jacketed in 0.127 mm thick copper foil and instrumented with standard polyimide backed constantan foil strain gages. During each of the experiments, axial and circumferential strains (ε_{11} and $\varepsilon_{\theta\theta}$) were measured along with the respective stresses σ_{11} and $\sigma_{\theta\theta}$. The effects of pressure on the strain gages were removed based on calibrations using identically instrumented samples of optical glass with known elastic constants. Importantly, the Berea samples used here were found to be very isotropic mechanically, as measured by comparing ε_{11} and $\varepsilon_{\theta\theta}$ during hydrostatic compression. Linear compressibilities were in agreement to within 5%.

MODERATE STRAIN EXPERIMENTS

The loading history of an exemplary experiment is illustrated in Figure 1. The experiment involves a sequence of perturbations in load subject to varying boundary conditions and executed from a series of initial stress conditions. At three different starting stress conditions, the axial stress and confining pressure

are controlled to produce perturbations in stresses enforcing the following boundary conditions: mean stress perturbations at constant differential stress (4 cycles of two different amplitudes), uniaxial stress perturbations (2 cycles), shear stress perturbations at constant mean stress (4 cycles of two different amplitudes), and uniaxial strain perturbations (4 cycles of two different amplitudes).

The mean and shear stress cycles are referred to here as *pure mode* owing to their direct link to equations 1a and 1b, while the uniaxial stress and uniaxial strain cycles are referred to as *mixed mode*, owing to the fact that they involve both mean and shear components. For an isotropic, linear elastic material, one should expect that, regardless of loading path, there should be a unique relationship between σ and κ as well as between τ and γ .

Figure 2 plots the volumetric strain as a function of the mean stress during the 2nd perturbation sequence (as shown in Figure 1). Considerable nonlinearity is apparent, reflected by hysteresis, curvature of stress strain curves, and deviations in stress-strain relationships for the different modes of deformation. The relationship between σ and κ as determined by the mean stress cycles does not describe the deformation during the other modes of deformation. Similarly, the relationship between τ and γ , as determined by the shear stress perturbations, does not describe the deformation during uniaxial stress and uniaxial strain. Thus, the data indicate that in general, it is not sufficient to superimpose simple rheologies describing \hat{K}_σ and \hat{G}_τ (i.e. \hat{K} and \hat{G} based on pure mode perturbations) to describe deformation during mixed mode loading paths.

We do however note some pattern to the stress-strain behavior shown in Figure 2. Note that the shear stress perturbation (at constant mean stress) causes an appreciable decrease in volumetric strain (i.e. a dilation). Accordingly, the uniaxial-stress and uniaxial-strain perturbations produce less volumetric strain (per unit change in mean stress) than is observed during the pure mean stress cycles. This suggests that a coupling term is required to handle volumetric strain resulting from changes in shear-stress. Similarly for the shear strain, a coupling term is required to handle the effects of mean stress changes on the shear rheology.

In many respects, the coupling terms appear relatively elastic (i.e. uni-valued functions of stress state), allowing for the potential to develop a general rheology by superposition of elastic coupling terms with hysteretic and stress dependent \hat{K}_σ and \hat{G}_τ . The development of a hysteretic rheology is beyond the scope of this paper†. In its place, a nonlinear elastic (non-hysteretic) approximation to the data is developed, which will prove useful as an illustration of the general character of the coupling terms. The rheology can be described by:

$$\Delta\kappa = \frac{\Delta\sigma}{\hat{K}_\sigma} + \Delta\tau \cdot \zeta(\sigma, \tau) \quad (3a)$$

$$\Delta\gamma = \frac{\Delta\tau}{\hat{G}_\tau} + \Delta\sigma \cdot \psi(\sigma, \tau) \quad (3b)$$

The terms ζ and ψ are the coupling terms. ζ handles the effects of changing shear stress on the mean stress rheology and ψ handles the effects of changing mean stress on the shear rheology.

While the form of the coupling terms is still not fully developed, reasonable behavior can be achieved using functionally similar forms for ζ and ψ :

$$\zeta = -A \tau^\alpha e^{-a\sigma} \quad (3c)$$

$$\psi = -B \tau^\beta e^{-b\sigma} \quad (3d)$$

Preliminary attempts to fit the Berea sandstone data lead to the following values: $\langle A \rangle \approx 1.8e-05 \text{ MPa}^{-(\alpha+1)}$, $\langle \alpha \rangle \approx 1.5$, $\langle a \rangle \approx 0.2 \text{ MPa}^{-1}$, $\langle B \rangle \approx 8.0e-06 \text{ MPa}^{-(\beta+1)}$, $\langle \beta \rangle \approx 1.0$, and $\langle b \rangle \approx 0.05 \text{ MPa}^{-1}$. Using these values, along with constant values of $\langle \hat{K}_\sigma \rangle = 10 \text{ GPa}$ and

† For the foundation of a hysteretic rheology, see *Boitnott [1993, 1996]; Guyer et al. [1995]*.

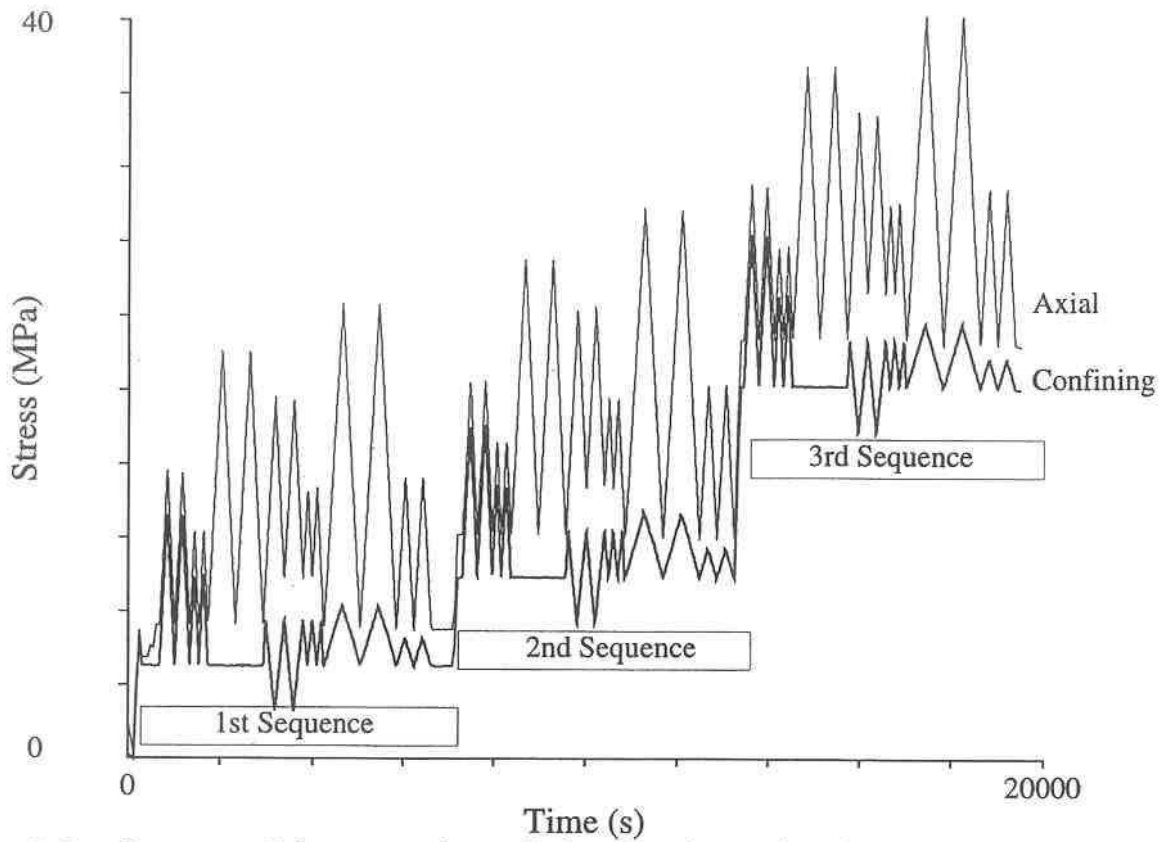


Figure 1: Loading protocol for an experiment designed to characterize the nonlinear rheology of rocks. A sequence of stress perturbations is repeated three times from three different starting stresses. Each sequence consists of perturbations in mean stress, uniaxial stress, shear stress, and uniaxial strain.

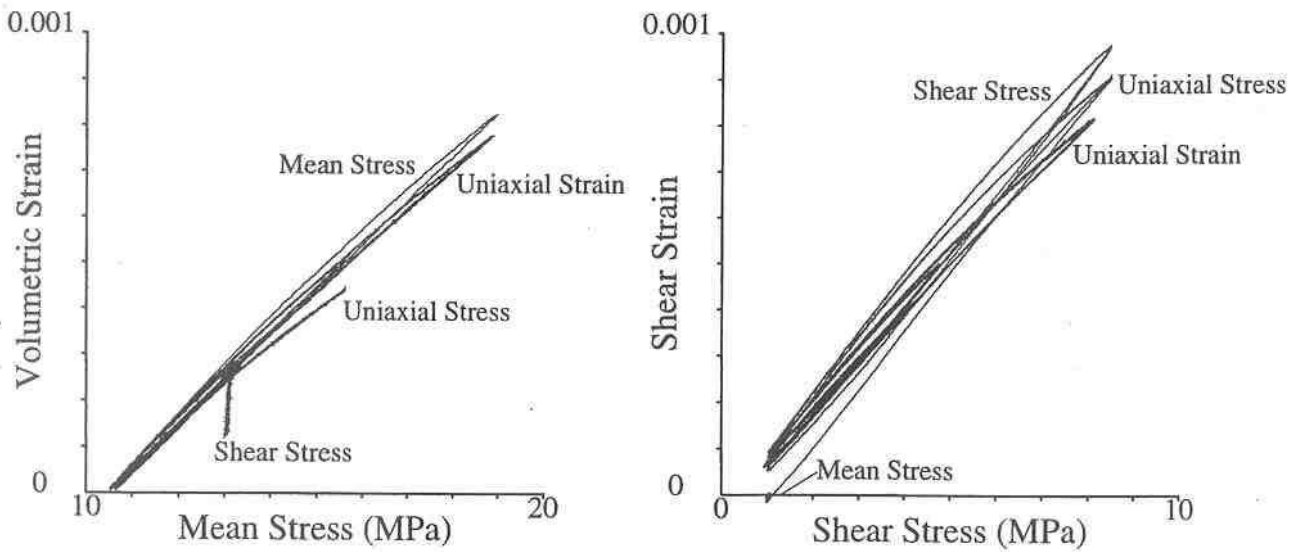


Figure 2: Stress versus strain data for the 2nd sequence in the loading history of Figure 1. Note that the shear stress cycle at constant mean stress causes a dilation, and that the stress versus strain relationships are different for the different modes of deformation.

$\langle \hat{G}_\tau \rangle = 8 \text{ GPa}$, model predictions for the data in Figure 2 are shown in Figure 3. Note that the non-linear model (equations 3a-d) reproduces the dominant features in the data, with the exception of the hysteresis which in this case has been explicitly ignored.

One underlying implication of the coupling terms is that inferred elastic moduli are a function of the loading path and the stress state from which they are derived. As an illustration, equations 3a and 3b can be rewritten as:

$$\hat{K} = \frac{\hat{K}_\sigma}{1 + r\hat{K}_\sigma\zeta} \quad (4a)$$

$$\hat{G} = \frac{r\hat{G}_\tau}{r + \hat{G}_\tau\psi} \quad (4b)$$

where r is the stress trajectory parameter ($r = \Delta\tau/\Delta\sigma$). Note that if r is positive, $\hat{K} > \hat{K}_\sigma$ and $\hat{G} > \hat{G}_\tau$ (since ζ and ψ are found to be negative).

COMPARISONS WITH "DYNAMIC" MODULI

The coupling terms described by equations 3c and 3d have been derived from moderate stress amplitude perturbations, and it remains unclear as to whether they result from stress (or strain) amplitude dependent phenomenon or if they are truly elastic in character. To begin addressing this issue a second testing protocol was developed which combines a complex loading history, static strain measurements, and ultrasonic velocity measurements. Compressional and shear velocities were measured using ultrasonic pulse propagation ($\approx 1 \text{ MHz}$) along the axis of the cores. As in the previous experiments, room dry Berea sandstone was used as the sample material. The addition of the velocity data provides information concerning the mechanical properties (i.e. moduli) for very small stress perturbations, and thus should provide constraints on the behavior of ζ and ψ in the limit of small strains.

The loading protocol is shown in Figure 4. After an initial loading and unloading of the confining pressure (to season the sample), confining pressure was increased to 50 MPa and velocities were measured at 5 points during the loading. The confining pressure was returned to 5 MPa, and a slight differential load (1 MPa) was applied. Confining pressure was then increased (at constant differential stress), stopping at the same 5 points for which velocities were measured during hydrostatic loading. At each of these 5 points during the loading, a series of stress perturbations was applied, consisting of perturbations in mean stress, uniaxial stress, and shear stress. Velocities were measured at various points during this loading sequence.

The observed nonlinearities in the static stress-strain relationships are quantitatively consistent with those from the moderate strain experiments discussed earlier. Stress-strain relationships during the mean stress and shear stress perturbations are used to infer $\langle \hat{K}_\sigma \rangle$ and $\langle \hat{G}_\tau \rangle$. Stress-strain relationships during the uniaxial stress perturbations are used to infer Young's modulus and Poisson's ratio ($\langle \hat{E}_{us} \rangle$ and $\langle \hat{\nu}_{us} \rangle$). In addition, velocities measured during the hydrostatic loading (events 1-5 in Figure 4) are used, along with the measured bulk density, to infer dynamic elastic constants controlling compressional and shear velocities (Y_v and G_v). Assuming isotropic, linear elasticity, these three sets of elastic constants were used to compute (infer) all other elastic constants. Thus there are three sets of inferred elastic constants, one inferred from pure mode perturbations, the second inferred from the mixed mode perturbation of uniaxial stress, and the third inferred from the compressional and shear velocities.

The inferred moduli are plotted in Figure 5. Comparing the results of the two static measurements, the expected systematic differences between elastic constants inferred using pure modes and those inferred from uniaxial stress are clearly seen. Most notably, inferred bulk modulus is higher for uniaxial stress than it is for the mean stress perturbation. This is the result of finite $\Delta\tau \cdot \zeta$ during the uniaxial stress perturbations. Inferred shear modulus is not notably different for the two cases, as is predicted by the non-linear rheology for these stress conditions.

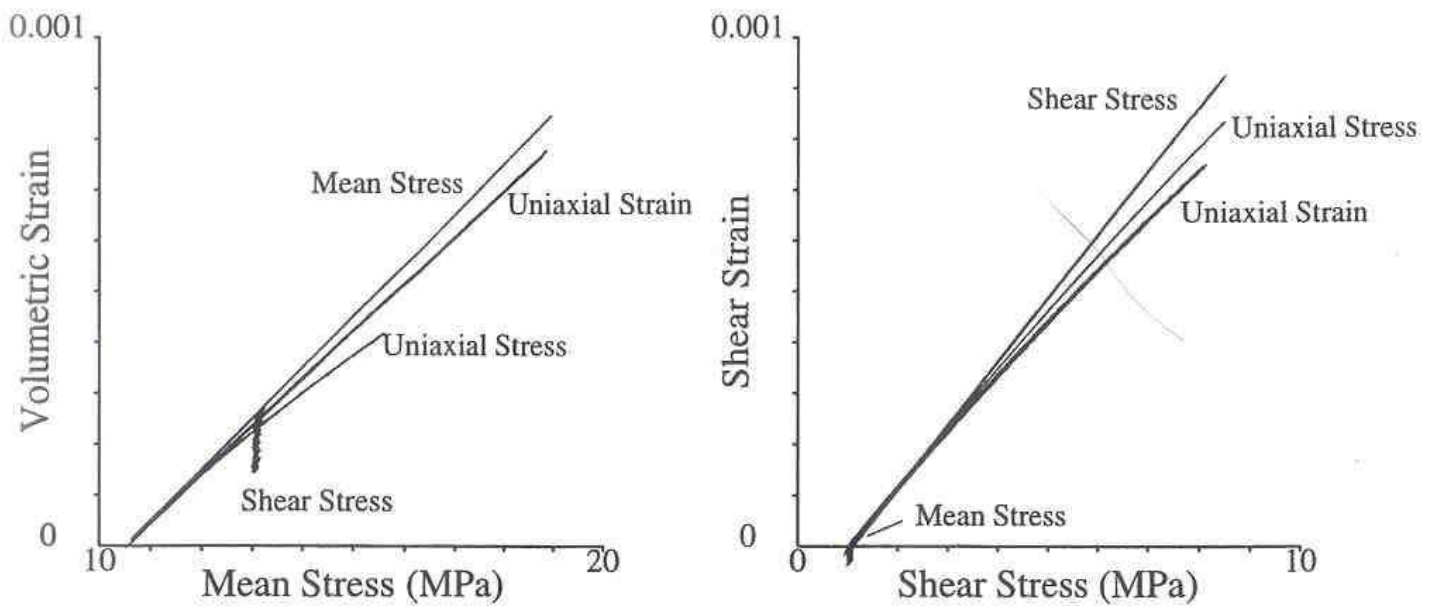


Figure 3: Predictions of the nonlinear elastic model for the data in Figure 2. Note the general agreement between the model (equations 3a-d) and the data for the entire loading sequence.

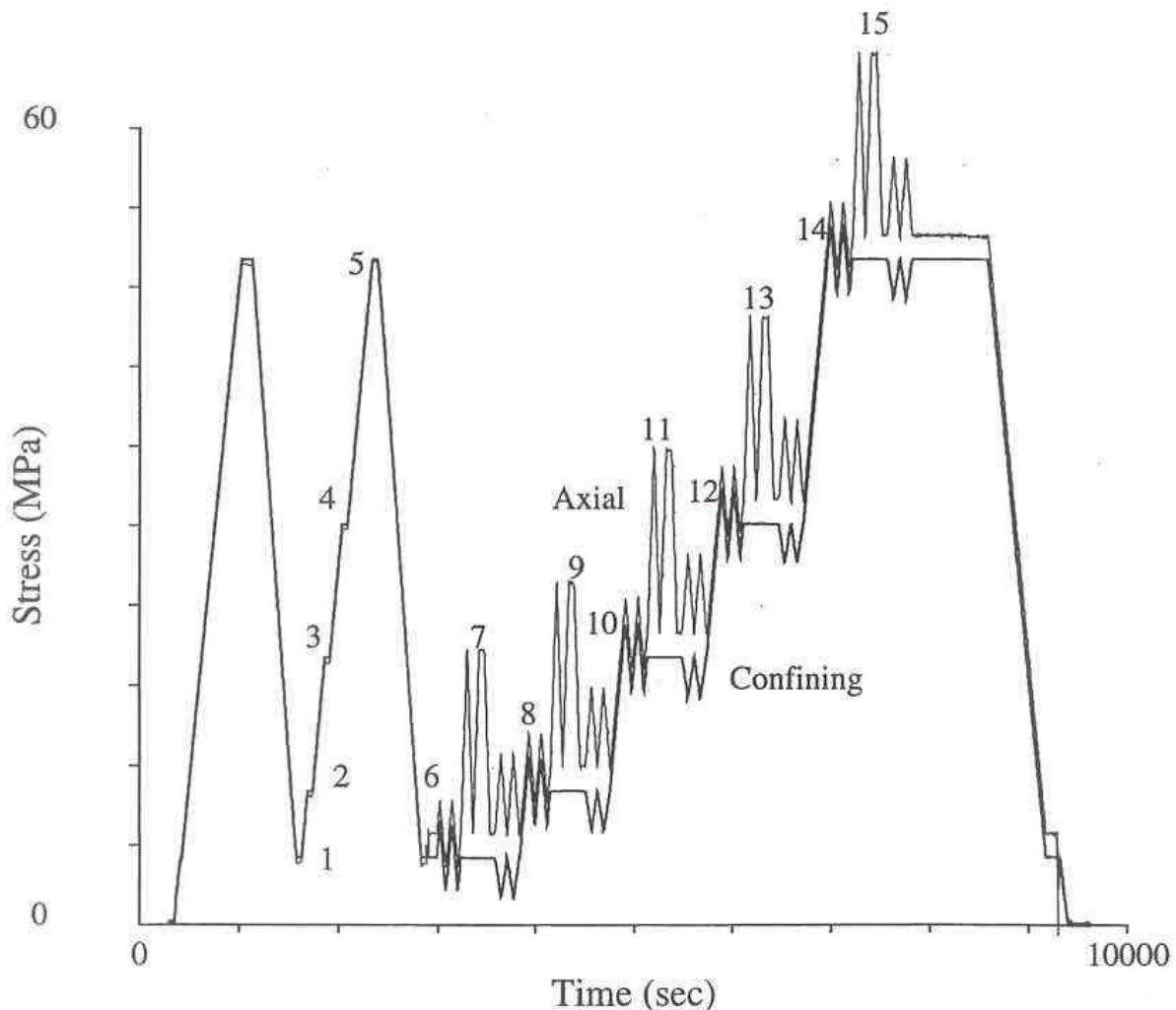


Figure 4: Loading protocol for a second experiment. Following two cycles in hydrostatic confining stress, as sequence of perturbations in stress is repeated five times from five different starting stresses. Perturbation sequences consisted of cycles in mean stress, uniaxial stress, and shear stress. Numbers indicates points in the loading sequence where ultrasonic velocities were measured.

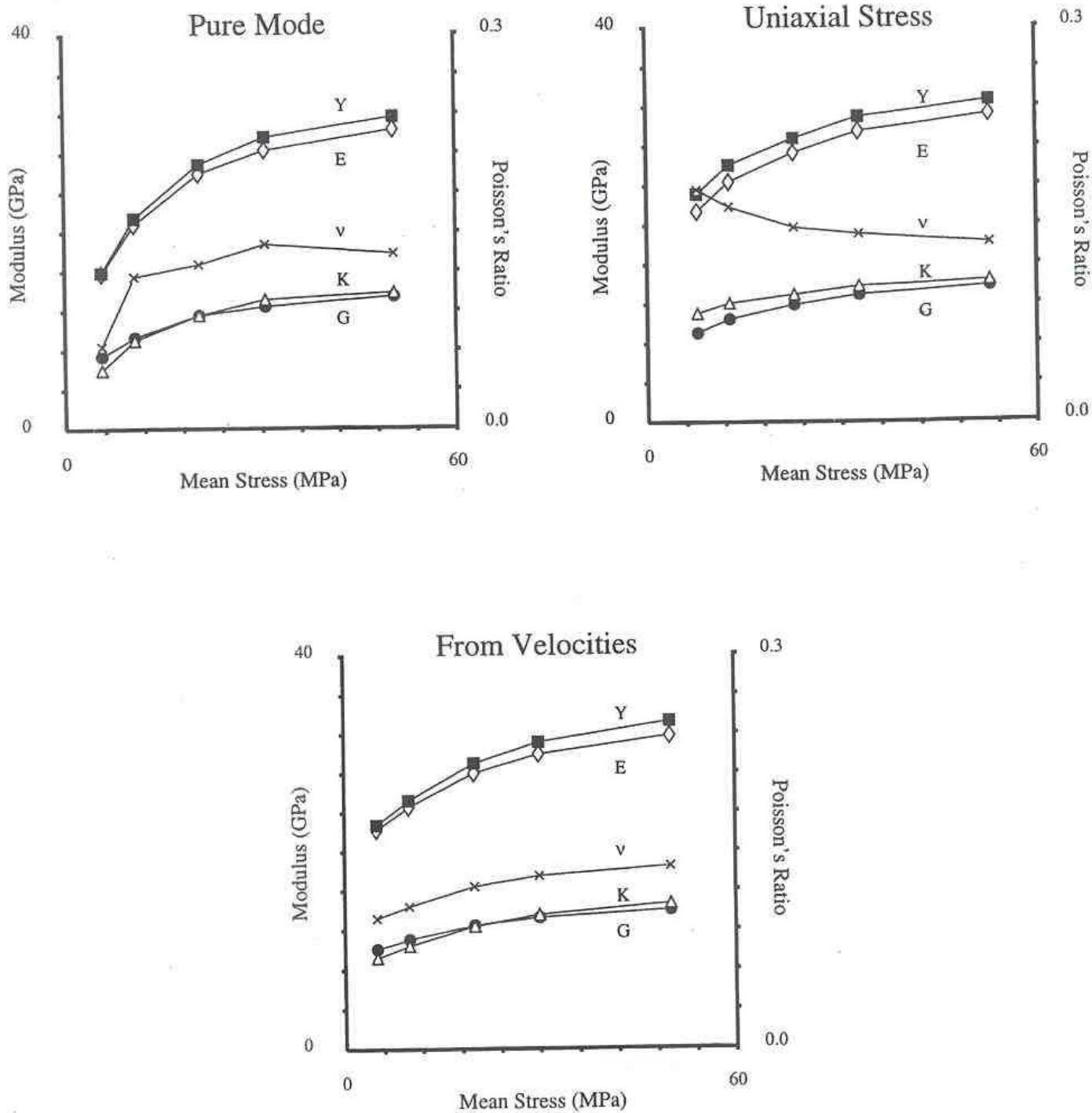


Figure 5: Inferred elastic constants determined from: a) [top left] pure mode measurements of $\langle \hat{K}_\sigma \rangle$ and $\langle \hat{G}_\tau \rangle$; b) [top right] measurements of $\langle \hat{E}_{us} \rangle$ and $\langle \hat{\nu}_{us} \rangle$ from uniaxial stress perturbations; and c) [bottom center] ultrasonic compressional and shear wave velocities under hydrostatic compression (i.e. points 1-5 in Figure 4).

Comparing these results with the moduli derived from the velocities, the statically determined moduli are in general lower. Importantly, the systematics between the K 's and G 's with respect to the mean stress are similar between the pure mode static and the velocity derived cases, and different for the mixed mode static case (uniaxial stress). This difference in systematics with mean stress is clearly reflected in the estimates of the v 's, which for isotropic, linear elasticity, is sensitive only to the ratio K/G .

CORRECTING FOR STRAIN AMPLITUDE

It has long been realized that the stress amplitude of the perturbations used to measure elastic constants strongly influences the measured values, and that this is one of the dominant causes of discrepancies between small amplitude dynamic measurements and larger amplitude static measurements (see for example *Walsh*, [1965]). Stress amplitude effects arise primarily from hysteretic nonlinearities. In the limit of small strains, hysteresis is minimized and it is found that inferred moduli (for a particular mode of deformation) approach the moduli at reversals in load observed during larger amplitude cycles (see *McCall et al.* [1996]). In order to better compare the static and dynamic data collected here, the local moduli \hat{K}'_{σ} , \hat{G}'_{τ} , \hat{E}'_{us} , and \hat{v}'_{us} at each reversal in loading direction were used in place of $\langle \hat{K}_{\sigma} \rangle$, $\langle \hat{G}_{\tau} \rangle$, $\langle \hat{E}_{us} \rangle$, and $\langle \hat{v}_{us} \rangle$. These stress amplitude corrected moduli were then compared with the dynamic moduli from the ultrasonic velocities. Results are plotted in Figure 6. The strain amplitude correction of the static moduli results in an elevation of the moduli with respect to their predecessors (i.e. static values in Figures 5a and 5b). Importantly, the amplitude correction has not changed the systematics between the K 's, G 's, and v 's with mean stress for either case. \hat{K}'_{σ} and \hat{G}'_{τ} from pure mode static measurements, compare favorably with K_v and G_v from the velocities, although velocity derived moduli are still slightly higher. G'_{us} is not significantly different from \hat{G}'_{τ} , but K'_{us} is notably higher than the inferences \hat{K}'_{σ} .

DISCUSSION

The experiments clearly demonstrate that the deformation of Berea sandstone is nonlinear. The data, along with a nonlinear elastic model which approximates much of the observed nonlinearity, illustrate that elastic moduli are dependent on the mode of deformation from which they have been measured. The most dominant effect in Berea sandstone is the ζ term, which acts to increase the bulk modulus (\hat{K}) during mixed mode loading paths where both mean stress and shear stress increase (or decrease) simultaneously.

The magnitude of the coupling terms ζ and ψ are found to decrease with increasing mean stress, and increase with increasing shear stress. They likely reflect, at least in part, shear stress (i.e. differential stress) induced anisotropy. As differential stress is increased, the stiffness to axial deformation is increased, thus resisting both volumetric and shear strains. In addition, the coupling terms may also reflect shear stress induced dilatancy, as grain and crack surfaces attempt to slide past opposing features.

There is some limited evidence that the stress induced anisotropy mechanism is the dominant process, as the coupling terms controlling moderate stress amplitude moduli (e.g. $\langle \hat{K} \rangle$ and $\langle \hat{G} \rangle$) also appear to control strain amplitude corrected moduli (e.g. \hat{K}' and \hat{G}'). Evidence of shear induced dilatancy is less clear, but is appealing in that dilatancy is known to occur at higher differential stresses. It is interesting to note that the nonlinear rheology presented in equations 3a-d predicts dilatancy (i.e. $\hat{K} < 0.0$) at high differential stresses. While extension to higher differential stresses will require higher order functions for ζ and ψ (as well as hysteresis in these terms), it is reasonable to expect that the rheology is extendible to these conditions.

The effects of the nonlinearities have many practical applications. The uniaxial stress path, which is commonly used to infer elastic constants, is strongly influenced by nonlinearities. Thus measurements of elastic constants from uniaxial stress tests (particularly those under unconfined or low confining stress) are not well suited for predictions of elastic constants for other modes of deformation. Inference of Poisson's ratio is one particularly clear example. In sandstones like Berea, it is commonly observed that Poisson's ratio, inferred from velocities measured as a function of confining pressure, increases with increasing confining pressure. The opposite effect is observed when Poisson's ratio is measured using uniaxial stress perturbations. This discrepancy is a direct result of the coupling terms being active during the uniaxial stress path.

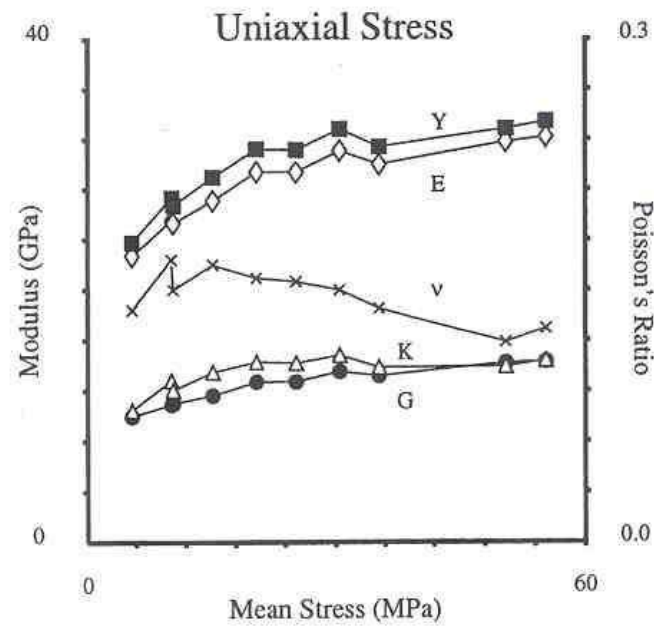
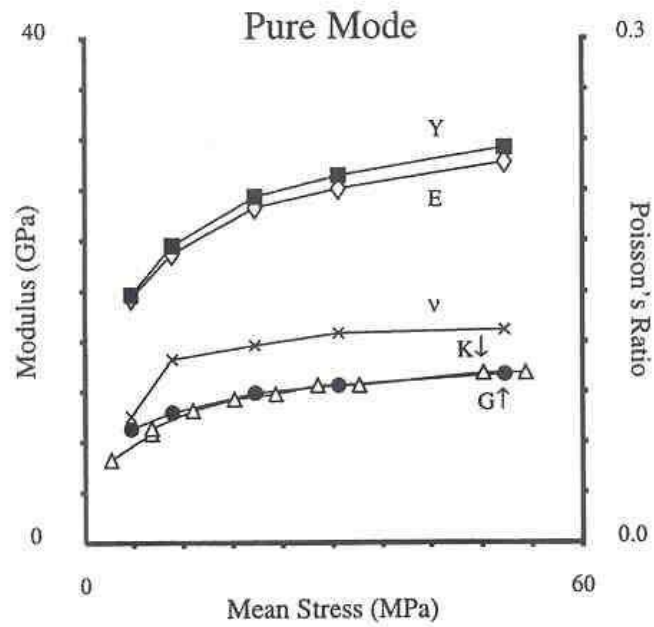


Figure 6: Inferred elastic constants determined from: (a) [top] pure mode measurements of \hat{K}'_{σ} and \hat{G}'_{τ} ; and (b) [bottom] measurements of \hat{E}'_{us} and $\hat{\nu}'_{us}$ from uniaxial stress perturbations.

ACKNOWLEDGEMENTS

This work was funded by AFOSR contract F49620-95-C-0019. The author thanks Peter Boyd and James Noel for help in performing the laboratory experiments.

REFERENCES

- Boitnott, G. N., (1993), Fundamental observations concerning hysteresis in the deformation of intact and jointed rock with applications to nonlinear attenuation in the near source region, in Proceedings of the Numerical Modeling for Underground Test Monitoring Symposium, Durango, Colorado, LA-UR-93-3839, p.121-134.
- Boitnott, G. N., (1996), Constructing a general rheological model for rock deformation, in Proceedings of the 18th Annual Seismic Research Symposium on Monitoring a Comprehensive Test Ban Treaty, 4-6 September, PL-TR-96-2153, p. 149-158.
- Gorbatsevich, F. F., (1996) Nonlinearity of strain in hard crystalline rocks, *Int. J. Rock Mech. Min. Sci. & Geomech. Abst.* v. 33, n. 1, pp. 83-91.
- Guyer, R. A., K. R. McCall, and G. N. Boitnott, (1995), Hysteresis, discrete memory, and nonlinear wave propagation in rock: a new paradigm, *Phys. Rev. Lett.*, v. 74, pp. 3491-3494.
- Johnson, P. A. K. R. McCall, and J. D. Meegan, (1993), Experimental and theoretical studies of spectral alteration in ultrasonic waves resulting from nonlinear elastic response in rock, in Proceedings of the Numerical Modeling for Underground Test Monitoring Symposium, Durango, Colorado, LA-UR-93-3839, p.107-120.
- Johnson, P. A., and P. N. Rasolofosaon, (1996), Nonlinear elasticity and stress induced anisotropy in rock, *J. Geophys. Res.*, v. 101, n. B2, pp. 3113-3124.
- McCall, K. R., R. A. Guyer, L. Zhu, G. N. Boitnott, L. B. Hilbert Jr., and T. J. Plona, (1996), Experimental determination of dynamic elastic properties of rock from quasistatic measurements, in *Rock Mechanics*, volume 1, A. A. Balkema, Rotterdam, Netherlands, pp. 147-154.
- Walsh, J. B., (1965), The effect of cracks on the uniaxial elastic compression of rocks, *J. Geophys. Res.*, v. 70, n. 2, pp. 399-411.